The simulation of the opposing fluxes of latent heat and CO2 over various land-use types: coupling a gas exchange model to a mesoscale atmospheric model

Boundary-Layer Meteorol (2011) 139:121–141
DOI 10.1007/s10546-010-9574-0

ARTICLE

The Simulation of the Opposing Fluxes of Latent Heat and CO_2 over Various Land-Use Types: Coupling a Gas Exchange Model to a Mesoscale Atmospheric Model

Mark Reyers · Andreas Krüger · Christiane Werner · Joaquim G. Pinto · Stefan Zacharias · Michael Kerschgens

Received: 22 December 2009 / Accepted: 7 December 2010 / Published online: 28 December 2010

Abstract A mesoscale meteorological model (FOOT3DK) is coupled with a gas exchange model to simulate surface fluxes of CO_2 and H_2O under field conditions. The gas exchange model consists of a C3 single leaf photosynthesis sub-model and an extended big leaf (sun/shade) sub-model that divides the canopy into sunlit and shaded fractions. Simulated CO_2 fluxes of the stand-alone version of the gas exchange model correspond well to eddy-covariance measurements at a test site in a rural area in the west of Germany. The coupled FOOT3DK/gas exchange model is validated for the diurnal cycle at singular grid points, and delivers realistic fluxes with respect to their order of magnitude and to the general daily course. Compared to the Jarvis-based big leaf scheme, simulations of latent heat fluxes with a photosynthesis-based scheme for stomatal conductance are more realistic. As expected, flux averages are strongly influenced by the underlying land cover. While the simulated net ecosystem exchange is highly correlated with leaf area index, this correlation is much weaker for the latent heat flux. Photosynthetic CO_2 uptake is associated with transpirational water loss via the stomata, and the resulting opposing surface fluxes of CO_2 and H_2O are reproduced with the model approach. Over vegetated surfaces it is shown that the coupling of a photosynthesis-based gas exchange model with the land-surface scheme of a mesoscale model results in more realistic simulated latent heat fluxes.

Keywords C3 single leaf photosynthesis · Latent heat flux · Net ecosystem exchange · Stomatal conductance · Sun/shade model

M. Reyers (✉) · A. Krüger · J. G. Pinto · S. Zacharias · M. Kerschgens
Institute for Geophysics and Meteorology, University of Cologne, Kerpener Str. 13,
50923 Cologne, Germany
e-mail: mreyers@meteo.uni-koeln.de

C. Werner
Experimental and Systems Ecology, University of Bielefeld,
Universitätsstr. 25, 33615 Bielefeld, Germany

1 Introduction

Conditions in the planetary boundary layer (PBL) and in particular its temporal evolution are characterised by very complex flow structures. Complexity is induced by several physical mechanisms working on different spatial and temporal scales (de Arellano et al. 2004; Adegoke et al. 2007; Fesquet et al. 2009). Beside advection and entrainment of air from the free atmosphere (Górska et al. 2008), the structure of the PBL is strongly influenced by turbulent surface fluxes of mass and momentum (e.g. Pielke and Niyogi 2009). Pielke and Avissar (1990) showed evidence of a significant impact of land-cover inhomogeneity on surface fluxes and on the structure of the lower atmosphere. Further, LeMone et al. (2007) detected a strong influence of vegetation cover on the horizontal distribution of surface fluxes using combined aircraft and tower data. In their study, maximum fluxes of sensible heat H and to a lesser extent minimum fluxes of latent heat LE were observed over sparse vegetation, while LE is naturally large over green vegetation. In previous years, many efforts have been made to accurately simulate these surface fluxes using numerical models (Shao et al. 2001; Heinemann and Kerschgens 2005; Mengelkamp et al. 2006; Beyrich and Mengelkamp 2006). The majority of meteorological models use a land-surface scheme proposed by Jarvis (1976), in which the parametrized transpiration of the plants only depends on meteorological variables (such as temperature, humidity and incident radiation). Nevertheless, it is well established that the physical process of plant transpiration is strongly linked to the physiological process of the photosynthetic CO_2 uptake through stomata (Zhan and Kustas 2001). Hence, CO_2 and energy exchanges should be coupled by the stomatal conductance for both CO_2 uptake and transpiration. Land-surface schemes that consider photosynthesis mostly reveal realistic fluxes of CO_2 and H_2O (e.g. Houborg and Soegaard 2004), with the schemes often driven with measured meteorological variables. Most mesoscale atmospheric models still use the Jarvis scheme (e.g. Xiu and Pleim 2001), while photosynthesis-based schemes are mainly applied in global climate studies (e.g. Sellers et al. 1996; Dai et al. 2003) or at the leaf and canopy scale (Werner et al. 2001; Collatz et al. 1991). Niyogi et al. (2009) pointed out the benefits of using photosynthesis-based schemes in mesoscale or weather forecast models, and they successfully replaced the Jarvis scheme with a photosynthesis-based scheme for simulations with a mesoscale meteorological model. As they developed the coupled gas exchange evapotranspiration model for a rather coarse horizontal resolution (10 km), a big leaf scaling procedure was applied. For higher resolution models and/or for canopies with deeper vegetation a more effective upscaling procedure is desired.

The present study is embedded in the framework of the Transregional Collaborative Research Centre 32 (TR32), which aims at analysing surface-atmosphere interaction processes on different spatial and temporal scales. In this study we couple a photosynthesis-based gas exchange model to the mesoscale meteorological model FOOT3DK with a horizontal resolution of up to 100 m. We determine how far the use of a photosynthesis-based stomatal model combined with a sun/shade scaling procedure leads to more realistic simulated latent heat fluxes when compared to the big leaf Jarvis scheme.

A description of the atmospheric, gas exchange, and the coupled models is given in Sect. 2. The general model set-up and the methods are described in Sect. 3, and Sect. 4 is dedicated to results from the coupled model, including simulated fluxes for single grid points, the opposing fluxes of CO_2 and H_2O over different land-use types, and simulations under anthropogenic elevated atmospheric CO_2 concentration. A short discussion is given in the final section.

2 Model Description

2.1 The Meteorological Mesoscale Model FOOT3DK

The prognostic model FOOT3DK (Flow Over Orographically structured Terrain 3-Dimensional, Kölner version) is a non-hydrostatic flow model using terrain following η-coordinates. Applied in a range of resolutions and domain sizes from the mesoscale γ down to the microscale α, the model is suitable for multiple passive nesting into itself or in suitable external models (Brücher 1997; Brücher et al. 2001), and has been used in many different applications. For example, Brücher et al. (1994a,b) used the model to derive a synthetic wind climatology over orographically structured terrain, while Pinto et al. (2009) reproduced wind storm situations over the North Rhine-Westphalia region. The dispersion of tracers, mostly within the context of the impact of traffic induced air pollution in a heavily inhabited area, were analysed e.g. by Brücher et al. (2001). Shao et al. (2001) used the model to estimate surface energy and momentum fluxes over heterogeneous orography, while Heinemann and Kerschgens (2005) compared different methods to compute the area-averaged surface energy fluxes in the context of the EVA-GRIPS Project (cf. Mengelkamp et al. 2006). Hübener et al. (2005) investigated evapotranspiration in a semi-arid environment, while Sogalla et al. (2006) studied rainfall and land-surface interactions. Detailed information on the model physics is given in Brücher (1997) or Shao et al. (2001). In all these applications, however, CO_2 fluxes have not been considered. Consequently, for this study FOOT3DK is coupled to a photosynthesis-based gas exchange model to estimate fluxes of CO_2 and H_2O over different land-use types.

The original land-surface scheme in FOOT3DK uses the classical big leaf approach following Jarvis (1976). It assumes that properties of the whole canopy can be reduced to that of a single sunlit leaf (Sellers et al. 1992), which has the same leaf area index (LAI) as the integrated canopy. The land surface scheme includes two soil layers, the first layer containing the upper 0.1 m of the soil, and the second layer reaching a depth of 1 m. At 1-m depth, the soil temperature and moisture are assumed to be constant on a time scale of a few days. The soil temperature is determined via the extended-force-restore-method (EFR-method, Jacobsen and Heise 1982). The prognostic equations of surface volumetric water content, mean volumetric water content, and the canopy intercepted water are solved following Noilhan and Planton (1989).

The surface energy budget is given by

$$G - Q - H - LE = 0, \tag{1}$$

where the ground heat flux G is calculated as a residual of the net radiation Q, sensible heat flux H, and latent heat flux LE, and thus contains the storage of energy.

Following Noilhan and Planton (1989), the latent heat flux LE over a surface grid cell includes the direct evaporation from fractional open water surfaces and from bare ground, the evaporation from intercepted leaf water and the transpiration of the plants. The transpiration (TR) is parametrized by a gradient approach:

$$TR = \frac{\delta_{veg}\left(1 - \delta_{wveg}\right)}{r_a + r_{st}} \left(q_{sat}\left(T_s\right) - q_a\right), \tag{2}$$

where $q_{sat}(T_s)$ is the saturated specific humidity at surface temperature T_s, and q_a is the specific humidity at the lowest atmospheric level, δ_{veg} is the vegetation covered fraction of the grid cell and δ_{wveg} is the fraction of vegetation covered with water. Beside the aerodynamical resistance r_a the transpiration rate is limited by the stomatal resistance r_{st}. A parametrization of the stomatal resistance r_{st} is given by

$$r_{st} = \frac{r_{s\,\min}}{LAI}\frac{F_1}{F_2 F_3 F_4}, \tag{3}$$

where r_{smin} is the plant specific minimal stomatal resistance and LAI is the leaf area index of the grid cell. Noilhan and Planton (1989) state that the stomatal resistance only depends on environmental variables, which are described by the functions $F_1 - F_4$. These functions represent the influences of photosynthetic active radiation (F_1), water stress that increases the plant sensitivity to stomatal closure (F_2), the response to water vapour pressure deficit (F_3) as a driving factor for transpiration, and the near-surface temperature (F_4). The value of F_2 is set close to zero when the soil moisture is below a plant specific wilting point, reflecting the effect that plants close their stomata under stress. See Noilhan and Planton (1989) for the specific forms and parameters used for $F_1 - F_4$. Note that, in this parametrization the photosynthetic molecular diffusivity of CO_2 is not taken into account in the computation of the stomatal resistance.

2.2 The Gas Exchange Model: Photosynthesis and Soil Respiration

The applied gas exchange model consists of two major components: a C3 single leaf photosynthesis model (Farquhar et al. 1980; as implemented by Ryel et al. 1993) and a sun/shade model (extended big leaf model; de Pury and Farquhar 1997), which scales leaf level processes to the canopy scale.

The model implementation of the single leaf photosynthesis of C3 plants of Farquhar et al. (1980) has been extensively described in the literature (e.g. Harley et al. 1992; Ryel et al. 1993; Werner et al. 2001). In short, it is based on ribulose-1.5-bisphosphate-carboxylase-oxygenase (Rubisco) kinetics of the catalysing enzyme as mediated by (i) the concentration of competing gaseous substrates, CO_2 and O_2, and (ii) the ratio of ribulose-1,5-bisphosphate (RuBP) concentration to enzyme active sites. The fundamental dependency is the response of net photosynthesis to leaf internal CO_2 partial pressure. At low CO_2 pressure, CO_2fixation is limited by the rate of fixation by Rubisco. After CO_2 fixation, RuBP has to be regenerated in the Calvin cycle that becomes the rate limiting step under high CO_2 concentration and is directly linked to the potential rate of electron transport since it requires energy from the light dependent reaction. The photosynthetic light response curve of a C3 plant follows a saturation curve, where the initial slope is equivalent to the light use efficiency (i.e. electron transport rate), while at the light saturation level the maximum carboxylation rate is reached.

The net photosynthesis rate A of a single leaf is consequently expressed as (see Harley et al. 1992; Beyschlag and Ryel 1999 for details):

$$A = \left(1 - \frac{0.5 o_i}{\tau c_i}\right) \min\left\{W_c, W_j\right\} - R_d, \tag{4}$$

where c_i and o_i are the partial pressures of CO_2 and O_2 in the intercellular air space, respectively, τ is the specificity factor for Rubisco, and R_d is the temperature dependent leaf dark respiration. W_c and W_j denote the limitations of photosynthesis due to either the availability of Rubisco or the RuBP regeneration, respectively:

$$W_c = \frac{v_{c\,\max} c_i}{(c_i + k_c(1 + o_i/k_o))}, \tag{5}$$

with $v_{c\ \max}$ being the maximum carboxylation rate at light saturation, and k_c and k_o are the Michaelis–Menten constants for carboxylation and oxygenation, respectively.

W_j is a function of the solar radiation (SR) induced electron transport within the leaf:

$$W_j = \frac{J c_i}{4\,(c_i + o_i/\tau)}. \tag{6}$$

The electron transport J is assumed to be proportional to the incident photosynthetically active radiation I (Harley et al. 1992):

$$J = \frac{\alpha I}{\sqrt{1 + \alpha^2 I^2 / J_{\max}^2}}, \tag{7}$$

where α is the quantum efficiency and J_{max} is the temperature dependent light saturated rate of electron transport.

The leaf CO_2 assimilation is directly controlled by the stomatal conductance to CO_2. The widely used empirical model of Ball et al. (1987) is applied, where the stomatal conductance g is linearly related to net photosynthesis A by

$$g = g_{\min} + b_1 A \frac{h_s}{c_s}, \tag{8}$$

where $g_{\min}$ denotes the plant specific minimal stomatal conductance, and h_s and c_s are the relative humidity and the mole fraction of CO_2 at leaf surface, respectively; b_1 is an empirical coefficient representing stomatal sensitivity to these factors.

Modelling the carbon fluxes of the entire canopy requires a scaling procedure from the leaf level to canopy scale. A very simple scaling procedure is the big leaf approach, which is known to be valid over short, open vegetation (e.g. grass) but tends to overestimate the photosynthetic CO_2 uptake of dense vegetation due to shading effects and diffuse light penetration in canopies with deeper vegetation (e.g. crop and forest; de Pury and Farquhar 1997). A more accurate scaling procedure for dense vegetation is an extended big leaf model, where the canopy is divided into sunlit and shaded fractions (de Pury and Farquhar 1997), accounting for the fact that, depending on the position of the sun, only a small fraction at the top of the canopy is fully sunlit, while deeper leaf layers often only absorb diffuse radiation. Accordingly, all functions in Eq. 1 are calculated for sun and shade leaf fractions separately, in order to compute the net photosynthesis rate for the sunlit fraction (A_{sun}) and the shaded fraction (A_{shade}). The LAI of the sunlit fraction (LAI_{sun}) is given by:

$$LAI_{sun} = \frac{1 - \exp\left(-LAI_c 0.5/\sin\beta\right)}{0.5/\sin\beta}, \tag{9}$$

where LAI_c is the leaf area index of the entire canopy and β is the solar elevation angle. The LAI of the shaded fraction (LAI_{shade}) can then simply be calculated as:

$$LAI_{shade} = LAI_c - LAI_{sun}. \tag{10}$$

The absorbed irradiance by the sunlit fraction I_{sun} consists of direct beam irradiance, diffuse irradiance, and scattered beam irradiance (I_b, I_d, I_{bs}, respectively):

$$I_{sun} = I_b + I_d + I_{bs}. \tag{11}$$

All three components depend on the solar elevation angle, the LAI of the entire canopy, and different coefficients of spectral absorption and reflection (de Pury and Farquhar 1997). The irradiance absorbed by the shaded fraction I_{shade} is calculated as a residual. A similar procedure is used for the calculation of the maximum carboxylation rate at light saturation of the sunlit fraction (v_{csun}) and the shaded fraction (v_{cshade}).

Table 1 Optimal respiration rates at 10°C for different land-use types following Bonan (1995)

Land use	a_3 (μmol m^{-2} s^{-1})
Forest	4.4
Grassland	1.7
Crop	2.5
Bare field	1.2
Water	0.0

The parameter a_3 refers to Eq. 14

Total canopy photosynthesis (A_c) is computed as the sum of the photosynthesis rates of both fractions (see de Pury and Farquhar 1997, for further details):

$$A_c = A_{sun} + A_{shade}. \tag{12}$$

The empirical model for the stomatal conductance (see Eq. 8) is applied for both fractions to calculate the stomatal conductance of the sunlit and the shaded fractions (g_{sun}, g_{shade}). As will be shown in the next subsection, g_{sun} and g_{shade} can be used to compute separate transpiration rates for both fractions.

For the computation of the net ecosystem exchange (*NEE*) the soil respiration R_s must be included:

$$NEE = A_c - R_s. \tag{13}$$

A simple parametrization for soil respiration of soils with different land uses has been proposed by Bunnell et al. (1977):

$$R_s = \left(\frac{w_s}{a_1 + w_s}\right)\left(\frac{a_2}{a_2 + w_s}\right) a_3 a_4^{(T-10)/10}, \tag{14}$$

where w_s and T denote the average soil water content and the soil temperature, respectively. Empirical factors are 50% capacity a_1 and saturation a_2. Additionally a temperature sensitivity parameter a_4 is introduced. Typical values for loamy soil are assumed ($a_1 = 0.20$, $a_2 = 0.23$, $a_4 = 2.0$; Bonan 1995), while the parameter a_3 is the surface type dependent optimal respiration rate at 10°C. Values for different land-use types are shown in Table 1.

2.3 The Coupled FOOT3DK/Gas Exchange Model

In the gas exchange model coupled to the mesoscale model FOOT3DK (hereafter abbreviated as the coupled model) the atmospheric parameters necessary for the simulation of *NEE* are supplied by the atmospheric component of FOOT3DK. In return, the simulated *NEE* of the gas exchange model is used to update the CO_2 concentration in the atmospheric component of FOOT3DK. As shown in Sect. 2.2, the gas exchange model also simulates the stomatal conductance for both the sunlit and the shaded fractions (g_{sun} and g_{shade}), separately. Net photosynthesis (A) is dependent on stomatal conductance, but A also limits the stomatal opening through its effect on leaf internal CO_2 partial pressure. Stomatal regulation of CO_2 exchange is inherently coupled to transpirational water loss, and to incorporate this link in the coupled model, the stomatal conductance of the gas exchange model is used in the land-surface scheme of FOOT3DK to simulate the transpiration of the canopies. By division of the canopy into sunlit and shaded fractions via the determination of their respective leaf area indices (LAI_{sun} and LAI_{shade}, see Eqs. 9 and 10) and the use of the according stomatal

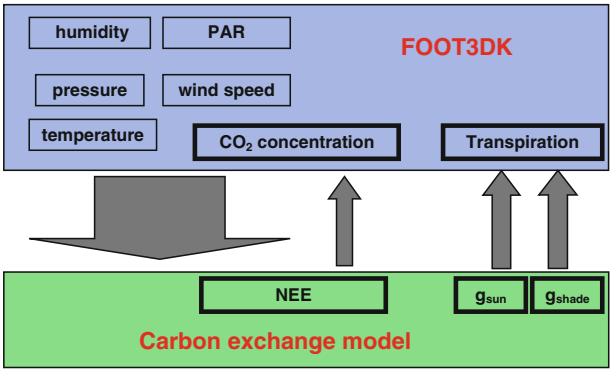

Fig. 1 Schematic illustration of the coupling of the gas exchange model with FOOT3DK

conductance (g_{sun} and g_{shade}), Eq. 2 can be applied to both fractions:

$$TR_{sun} = \frac{\delta_{veg}\left(1-\delta_{wveg}\right)}{r_a + 1/g_{sun}} \left(q_{sat}\left(T_s\right) - q_a\right) \frac{LAI_{sun}}{LAI_c}, \tag{15}$$

$$TR_{shade} = \frac{\delta_{veg}\left(1-\delta_{wveg}\right)}{r_a + 1/g_{shade}} \left(q_{sat}\left(T_s\right) - q_a\right) \frac{LAI_{shade}}{LAI_c}. \tag{16}$$

The transpiration of the entire canopy (TR_c) is then computed as the sum of the transpiration rates of both fractions:

$$TR_c = TR_{sun} + TR_{shade}. \tag{17}$$

A simplified illustration of the coupling procedure of FOOT3DK with the carbon exchange model is shown in Fig. 1. In its standard version FOOT3DK provides the atmospheric parameters: surface pressure, temperature, relative humidity, and wind velocity. For the gas exchange model variables from the lowest model level h_0 are relevant, where this level is defined at each grid point as:

$$h_0 = z_0 + z_d, \tag{18}$$

where z_0 is the aerodynamic roughness length and z_d is the zero-plane displacement.

Photosynthetically active radiation (PAR) can be calculated from the simulated incoming solar radiation (SR). The ratio of PAR to SR for certain areas has been reported in many studies. For example, the ratio ranges from 0.47 to 0.51 for Cambridge, U.K. (Szeicz 1974), and from 0.47 to 0.5 for Copenhagen, Denmark (Kvifte et al. 1983). For our simulations we have tested different ratios of SR to PAR, and a ratio of 0.47 shows best agreement between simulated PAR and measurements performed in the investigation area (not shown).

3 Model Set-Up and Methods

Simulations of the coupled model have been performed with a horizontal resolution of 100 m. The model domain is located in the surrounding of Selhausen (50.865°N, 6.436°E), a rural area located between Aachen and Cologne, North-Rhine-Westphalia, Germany (see Fig. 2), which features heterogeneous land-use types. The model domain comprises a terrain of 65 (95) grid points in the west-east direction and 74 (90) grid points in the south-north direction

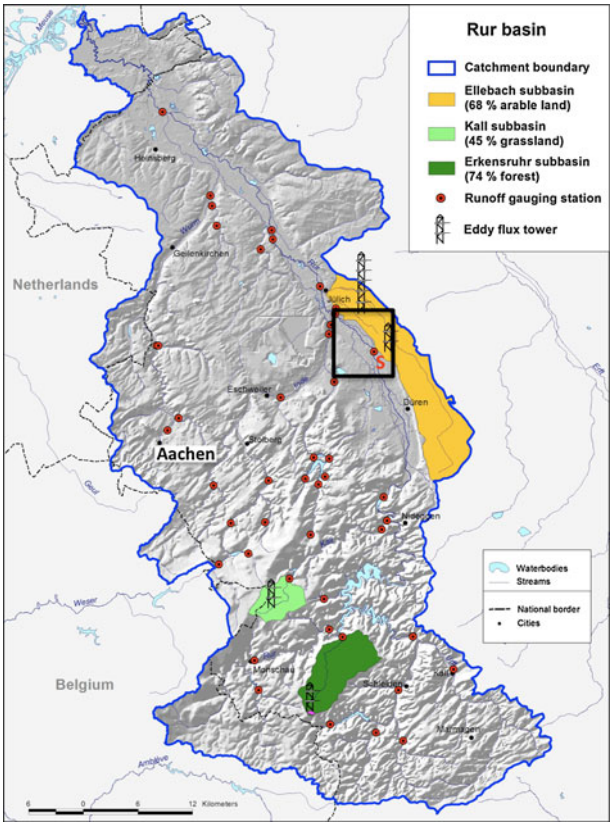

Fig. 2 Rur catchment basin. The *black box* denotes the simulation area, "S" the village Selhausen

for simulations of the year 2008 (2009). Eight land-use types have been selected, which originate from an ASTER (Advanced Spaceborne Thermal Emission and Reflection Radiometer) land-use classification (e.g. Waldhoff 2010). FOOT3DK is nested in the mesoscale prognostic model COSMO-LM (Baldauf et al. 2009) with a resolution of 2.8 km × 2.8 km, which has been forced with analyses from the COSMO-DE model of the German Weather Service (Deutscher Wetterdienst DWD). Using a triple one-way passive nesting (1 km, 250 m, 100 m), a resolution of up to 100 m is achieved (Brücher 1997, see also Sect. 2.1). The 1-km simulations commence at 0300 UTC and are initialised with output variables of the COSMO-LM simulations (e.g. soil moisture, soil temperature, humidity, air temperature, etc.). The 250-m (100-m) simulations are initialised with the output of the 1-km (250-m) simulations at 0400 UTC (0500 UTC). Since this is the first study to consider CO_2 fluxes within the context of FOOT3DK, atmospheric CO_2 concentration is not a standard output variable. Therefore, FOOT3DK is initialised with pre-defined CO_2 concentrations, which are estimated from vertical profiles of airborne measurements. These measurements have been performed in the area near Selhausen up to a height of 1600 m. Above this altitude, a constant background CO_2 concentration of 386 μmol mol^{-1} is assumed, while near-surface concentrations of more than 400 μmol mol^{-1} have been observed. An essential input parameter for the simulations is the LAI. Values for the LAI of wheat and sugar beet have been scanned

by a LICOR-3000A area meter. For other plant and land-use types reported values from the literature have been used.

Simulated fluxes of CO_2 and H_2O are compared to eddy-covariance measurements for several days during the spring and summer of 2008 and 2009. The eddy-covariance sensors (CSAT3 3-D sonic anemometer and a LI7500 infrared gas analyser) are mounted over a 190 m × 60 m wheat field and a 178 m × 237 m sugar beet field near Selhausen. The turbulent fluxes were measured at 1.6 m (wheat) and 2.2 m (sugar beet) height above the ground, while meteorological variables (e.g. humidity, temperature, etc.) have been quantified at 2 m above the ground. A detailed methodological description of the eddy-covariance flux measurements can be found in Graf et al. (2010a,b).

4 Results

4.1 Verification of the Gas Exchange Model

The stand-alone version of the sun/shade gas exchange model described in Sect. 2.2 is evaluated by comparing simulated CO_2 fluxes with eddy-covariance measurements. Simulations are driven with measured physiological and atmospheric variables (see Sect. 3). Simulated 30-min averaged daily plots of the *NEE* for four days are plotted against their corresponding observations in Fig. 3. Despite some bias, the carbon exchange model shows no systematic error. The magnitudes and the general diurnal features are simulated realistically for all four days.

The characteristic variability of the net ecosystem exchange is generally induced by variations in incident light intensities (due to the solar elevation angle or to the presence or absence

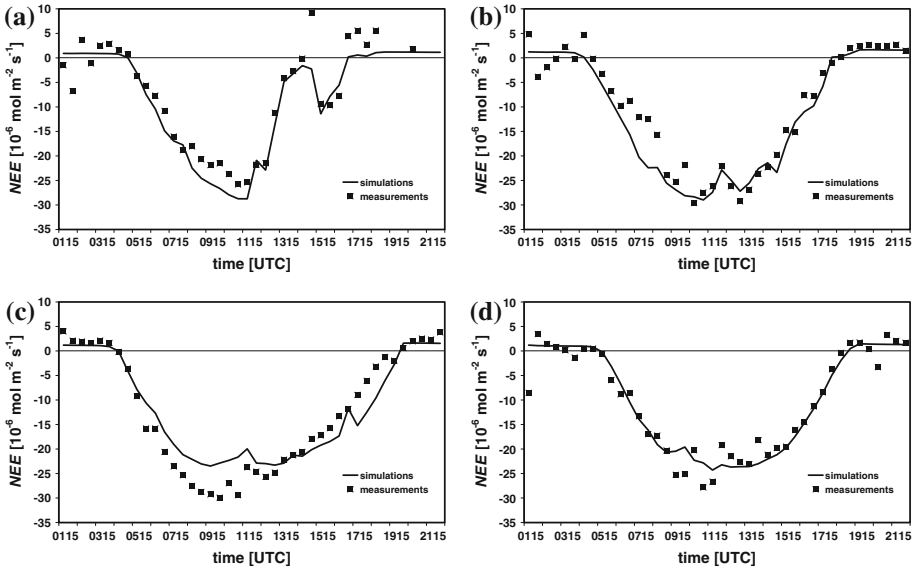

Fig. 3 30-min averaged simulated and measured net ecosystem exchange (*NEE*) for **a** 23 April 2008, wheat, **b** 06 May 2008, wheat, **c** 01 July 2008, sugar beet, and **d** 21 April 2009, wheat. *Negative values* indicate fluxes from atmosphere into plants and vice versa. This is valid for all following figures

of clouds). For example, a strong weakening of the *NEE* after midday on 23 April 2008 was caused by clouds emerging after sunny periods during the morning. This effect is indeed well reproduced with the gas exchange model (cf. Fig. 3a). On 6 May 2008 the net ecosystem exchange decreased in absolute value around midday, and this decrease, which is caused by a short cloudy period, is captured by the model as well.

In summary, simulated fluxes of CO_2 from the stand-alone version of the gas exchange model correspond well with field measurements when the model is driven with realistic atmospheric input parameters. In the coupled model input variables are provided by the atmospheric component of FOOT3DK (cf. Sect. 2.3).

4.2 Simulation of Fluxes with the Coupled Model

The results of the coupled model are presented for three exemplary days (23 April 2008, 1 July 2008, and 24 April 2009). Figures 4, 5 and 6 show the simulated daily plots of net ecosystem exchange (*NEE*) and latent heat flux (*LE*) over single grid points with wheat and

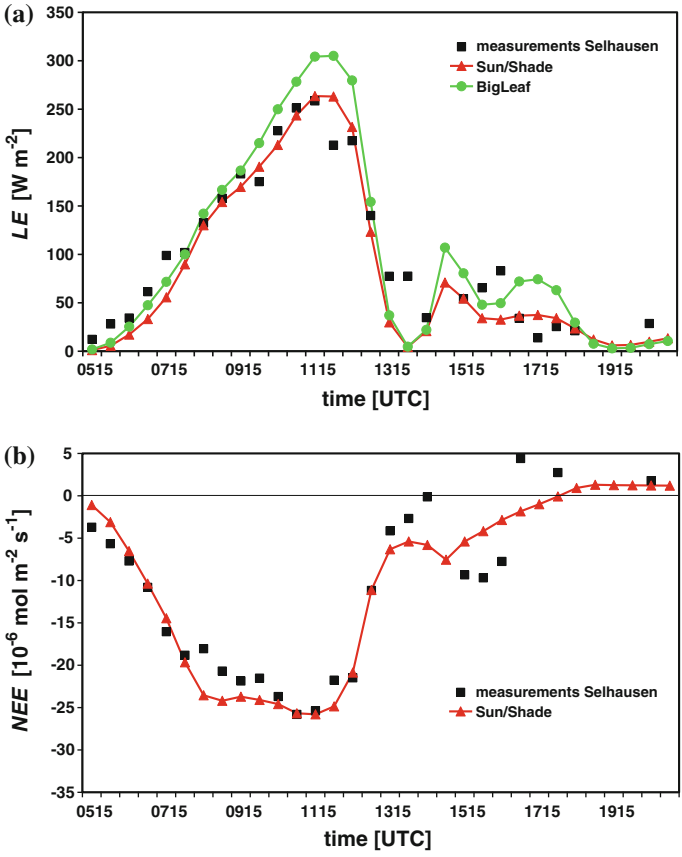

Fig. 4 30-min averaged measured (*dotted lines*) and simulated fluxes (*solid lines*) of grid points with wheat for 23 April 2008. **a** Latent heat flux (*LE*), *green line* corresponds to simulations with the standard big leaf approach, *red line* to simulations with the coupled sun/shade model (for details see text). **b** Net ecosystem exchange (*NEE*)

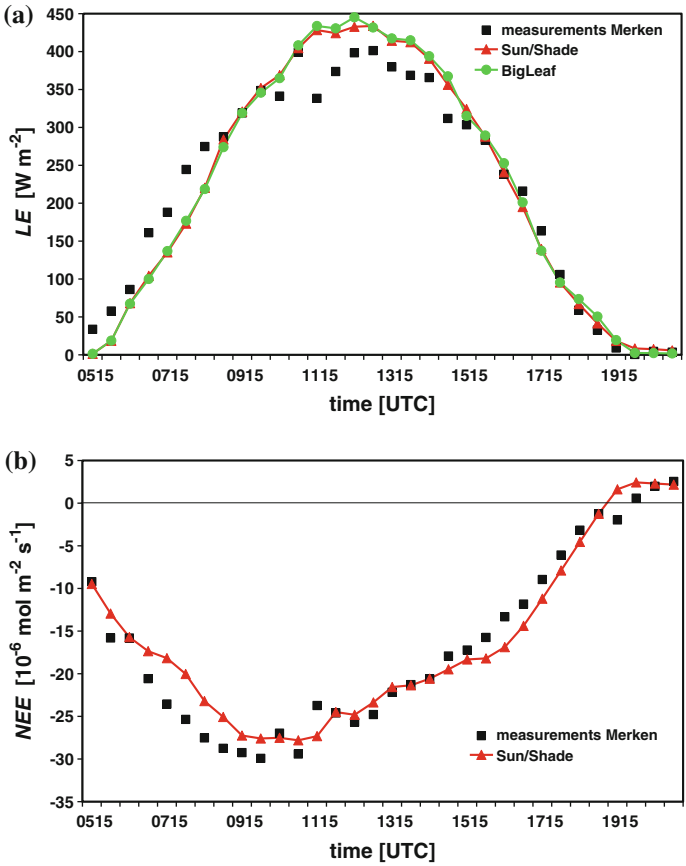

Fig. 5 As Fig. 4, but for sugar beet at 1 July 2008

sugar beet and their corresponding observations for these days. In addition, simulated latent heat fluxes obtained with the original big leaf approach are also included in Figs. 4a, 5a, 6a to illustrate the benefit of a photosynthesis-based land-surface scheme in the coupled model. While the latent heat flux is mostly overestimated using the original big leaf approach, the photosynthesis-based simulations of the coupled model are more realistic.

On 23 April 2008 (Fig. 4) simulated *LE* and *NEE* of the coupled model closely follow the observations until early afternoon, while the big leaf approach clearly overestimates the latent heat flux. After 1300 UTC simulations obviously differ from measurements to some extent. For example, the local maxima (in absolute values) in the measurements of net ecosystem exchange and latent heat flux in early afternoon are caused by a short cloudless period, which is simulated too early. Nevertheless, evidence is provided that in a fair weather situation FOOT3DK produces realistic atmospheric variables, as required by the gas exchange model.

The simulated latent heat flux in the coupled model is similar to values obtained with the big leaf approach for 1 July 2008 (Fig. 5a). A possible cause for the small differences between both approaches is a limitation in the stomatal conductance by a maximum value in both model versions: under strong incident radiation the stomatal opening is limited to prevent dehydration of the plants. However, and despite underestimated fluxes in the

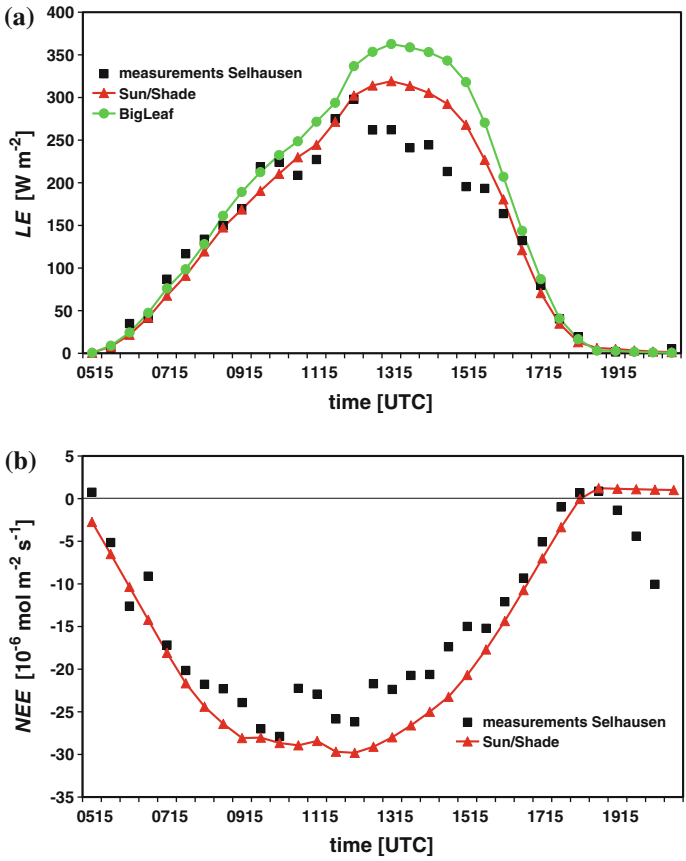

Fig. 6 As Fig. 4, but for wheat at 24 April 2009

morning and slightly overestimated fluxes during the day, both the coupled model and the big leaf approach simulate quite realistically the latent heat fluxes. The simulated net ecosystem exchange closely follows the corresponding observations. As well as the magnitudes, the general course of the day is captured well by the coupled model.

On 24 April 2009 the simulated latent heat flux in the big leaf approach is clearly overestimated, while simulations of the coupled model are in good agreement with observations until 1200 UTC. The decline in the measurements after midday is not detected by the model. We have not found a reason for this decline, because no significant alterations are observed in the measured meteorological variables after midday. The model-predicted net ecosystem exchange is slightly overestimated in absolute values during the day, but nevertheless the simulated general course of the day matches the observations.

After evaluating the results of the coupled model for single model grid points, opposing fluxes of CO_2 and H_2O over different land uses are investigated. The model domains of the simulations are presented in Fig. 7a (23 April 2008, and 1 July 2008) and Fig. 7b (24 April 2009). Please note that brown surfaces in Fig. 7a correspond to bare field for 23 April 2008 (unvegetated sugar beet fields before growing season), while these surfaces represent sugar beet fields for 1 July 2008. Horizontal spatial distributions of latent heat flux and net

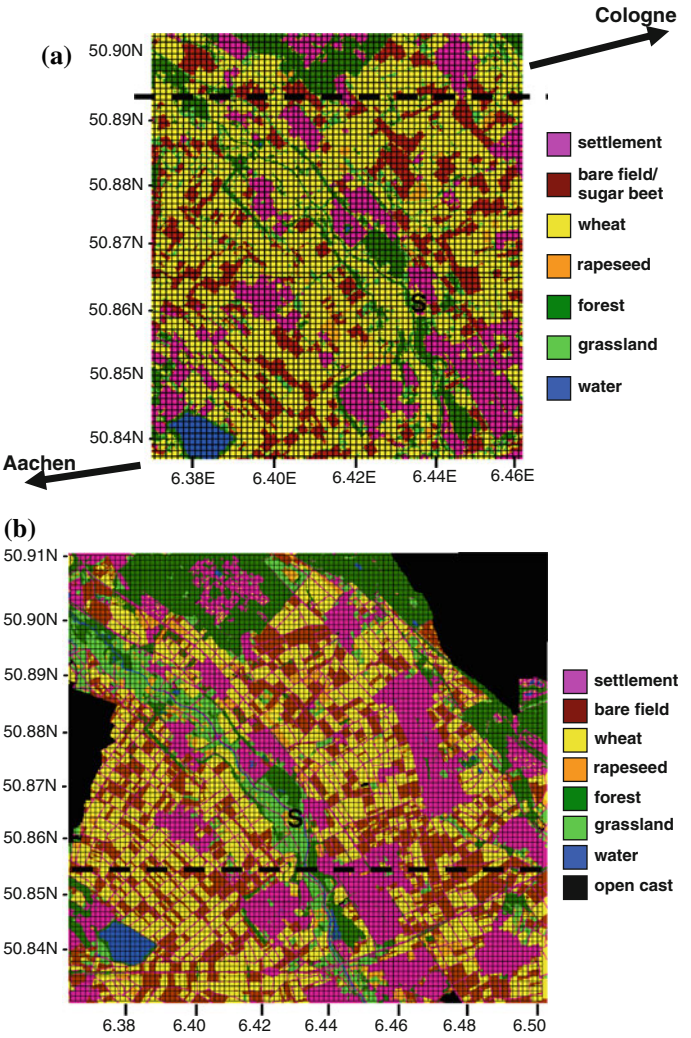

Fig. 7 Model domains for the simulations of **a** 2008 (23 April and 1 July) and **b** 2009 (24 April). "S" denotes the location of Selhausen. Please note that in **a** *brown surfaces* correspond to bare field for 23 April 2008, while for 1 July 2008 these surfaces represent fields with sugar beet. The *dashed lines* refer to transects in Figs. 8, 9, 10

ecosystem exchange for the entire model domain reveal that both fluxes are clearly related with the underlying land-use type (not shown). Figure 8 shows the hourly-averaged (1100–1200 UTC) simulated *LE* and *NEE* over the 65 grid points along the black dashed line in Fig. 7a for 23 April 2008. Both fluxes are highest (in absolute values) over grid points with crop, while small fluxes are observed for grid points with bare field. Aside from transpiration, the direct soil evaporation is taken into account in the latent heat flux. Therefore, comparable high latent heat fluxes are simulated for bare field compared to *NEE*, which is close to zero for these grid points. Since both fluxes are thus somewhat decoupled, a merely moderate anticorrelation between net ecosystem exchange and latent heat flux is observed

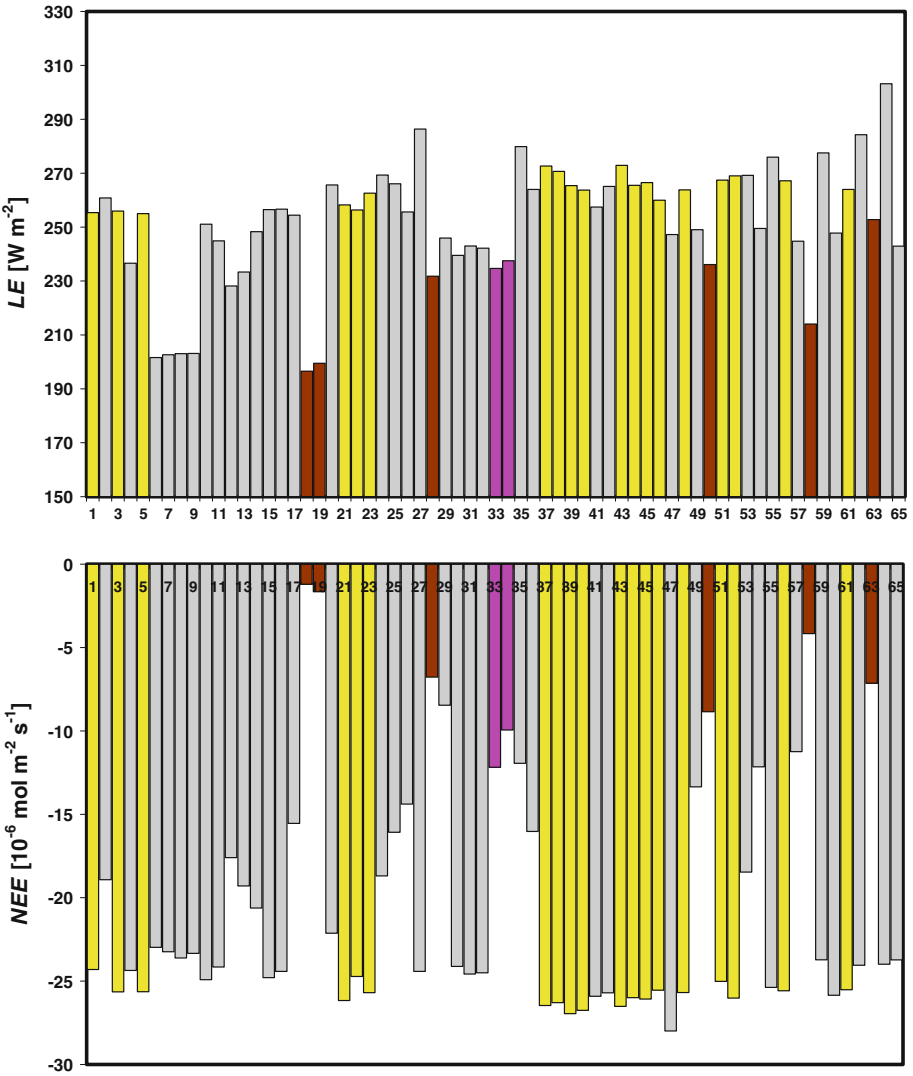

Fig. 8 1-h averaged (1100–1200 UTC) simulated latent heat fluxes (*LE, upper panel*) and net ecosystem exchange (*NEE, lower panel*) for 23 April 2008. Shown are values at the 65 grid points across the *black dashed line* in Fig. 7a. *Negative values* mean fluxes from atmosphere to surface and vice versa. Grid mashes with a dominant land-use type (>80%) are depicted with the same land use *colours* as in Fig. 7a (*yellow* wheat; *brown* bare field; *magenta* settlement). Grid mashes without a dominant land-use type (<80%) are *coloured grey*

($r = -0.44$). In addition to soil characteristics, the fluxes are mainly determined by the LAI of the different land-use types, in particular the net ecosystem exchange. A very high spatial correlation between the LAI and 1-h averaged simulated net ecosystem exchange is found for the entire model domain ($r = 0.9$). The correlation between the LAI and 1-h averaged simulated latent heat flux is comparably small ($r = 0.34$).

In Fig. 9, 1-h averaged simulated net ecosystem exchange and latent heat flux along the black dashed line in Fig. 7a are presented for the 01 July 2008. The variability of both *NEE*

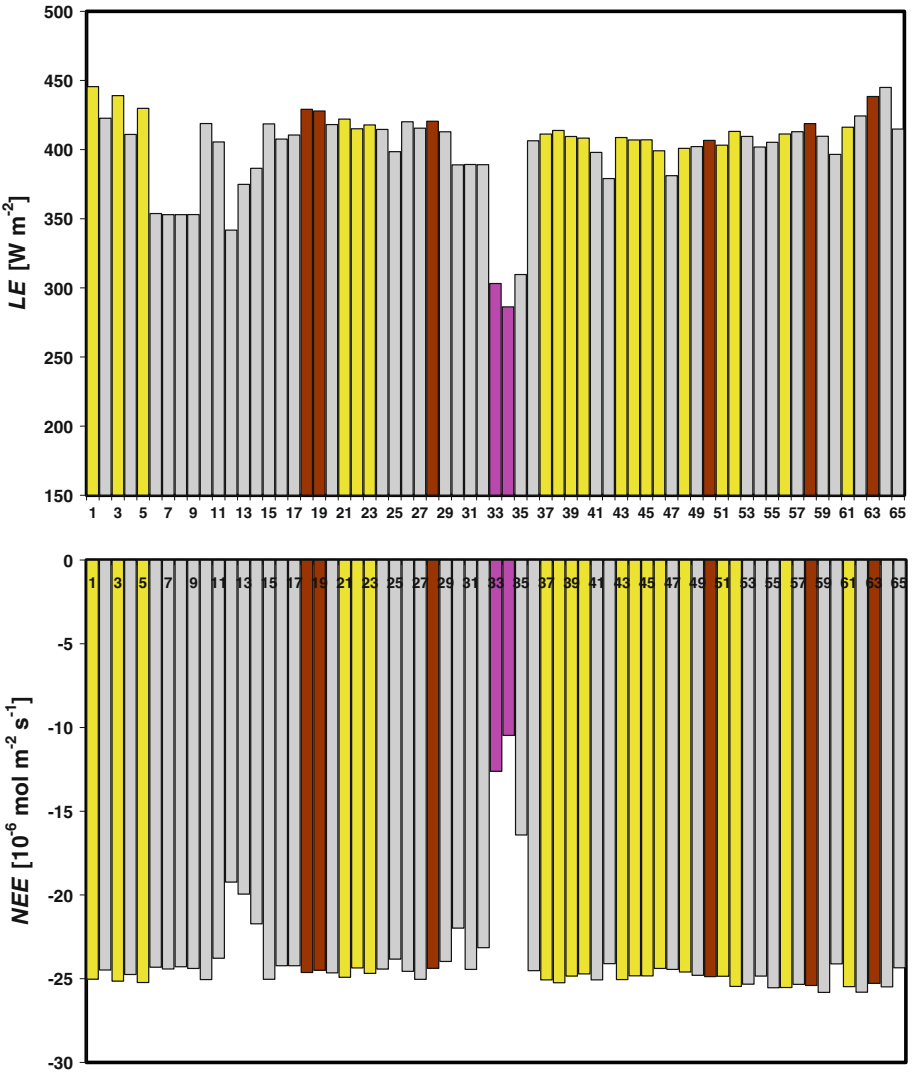

Fig. 9 As Fig. 8, but for the 1 July 2008. Grid mashes with a dominant land use type (>80%) are depicted with the same land use *colours* as in Fig. 7a (*yellow* wheat; *brown* sugar beet; *magenta* settlement). Grid mashes without a dominant land-use type (<80%) are *coloured grey*

and *LE* is weak compared to 23 April 2008, as the unvegetated fields in April are now covered with sugar beet. Therefore, simulated latent heat flux and net ecosystem exchange over grid points representing these fields are similar to simulated fluxes over grid points with wheat. Small fluxes only occur over grid points dominated by settlement. Due to these surface features a high spatial anticorrelation between the fluxes presented in Fig. 9 is observed ($r = -0.81$).

Unlike the measurements, the model enables the quantification of the single components of the simulated latent heat flux (e.g. transpiration and evaporation). Figure 10 shows 1-h averaged (1100–1200 UTC) simulated net ecosystem exchange and transpiration rates over

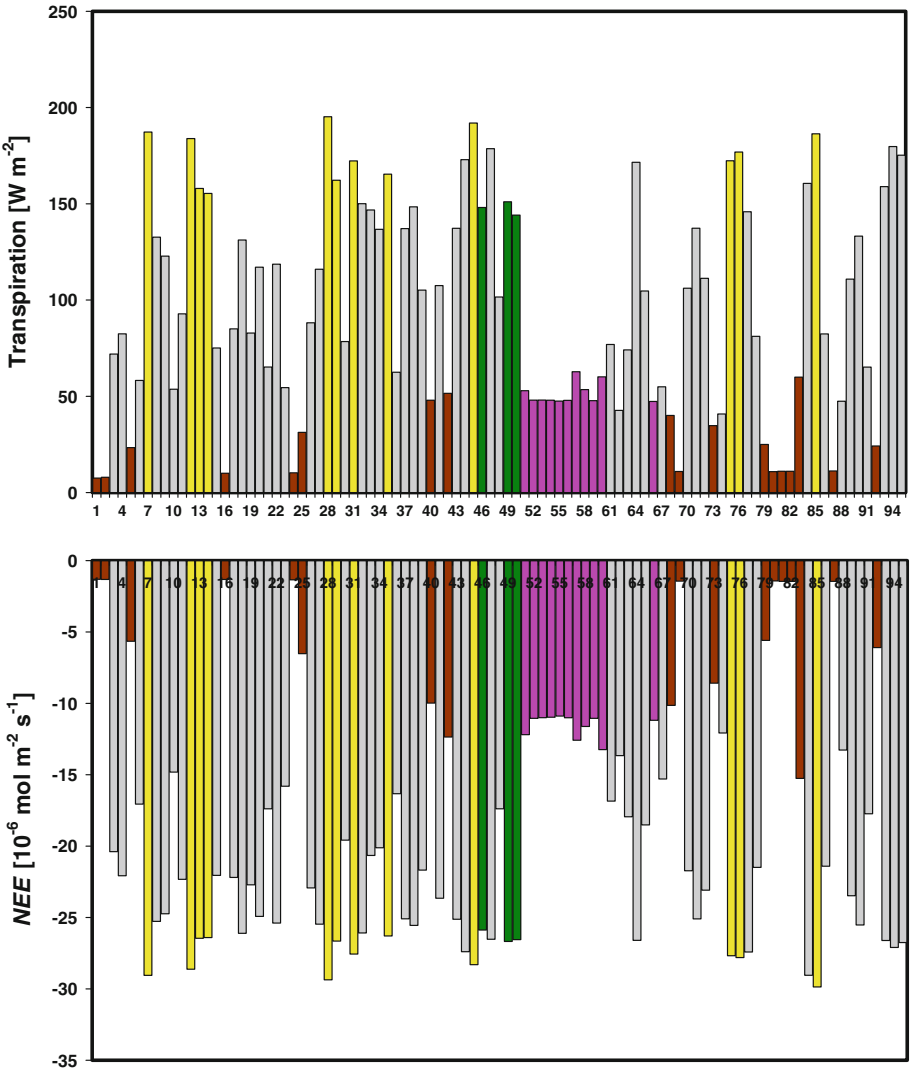

Fig. 10 1-h averaged (1100–1200 UTC) simulated plant transpiration (*upper panel*) and net ecosystem exchange (*NEE, lower panel*) for the 24 April 2009. Shown are values at the 95 grid points across the *black dashed line* in Fig. 7b. Grid mashes with a dominant land-use type (>80%) are depicted with the same land use *colours* as in Fig. 7a (*yellow* wheat; *brown* bare field; *magenta* settlement; *green* forest). Grid mashes without a dominant land-use type (<80%) are *coloured grey*

the 95 grid points along the black dashed line in Fig. 7b for 24 April 2009. Both fluxes show a high spatial variability. Again, highest fluxes are observed over grid points dominated by crop. Both transpiration and net ecosystem exchange are close to zero over bare field, while slightly higher fluxes are found for grid points with settlement (since a sealing of only 50% is assumed for this type of land use). The fluxes presented in Fig. 10 are highly anticorrelated ($r = -0.93$), thus demonstrating the pronounced effect that the transpirational water loss and the photosynthesis of the plants are linked via stomatal opening.

Similar results are found for 23 April 2008 and for 1 July 2008 ($r = -0.96$ and $r = -0.94$, respectively).

4.3 Sensitivity to Atmospheric CO_2 Concentration

It is well established that plants regulate their transpirational water loss in relation to carbon gain by a reduction in stomatal conductance in the presence of elevated CO_2 concentrations (Tricker et al. 2005; Garcia-Amorena et al. 2006). We now investigate whether the coupled model is able to reproduce this behaviour. For this purpose, in the simulation of the 23 April 2008 we elevated the initialising CO_2 concentration by 300 μmol mol^{-1}. An increase of CO_2 of about 300 μmol mol^{-1} refers to the assumptions of moderate climate scenarios of anthropogenic atmospheric CO_2 increase by the year 2100 (SRES-A1B scenario). As a result, the enhanced CO_2 supply and thus higher internal CO_2 concentration results in an increased carbon assimilation and thus in a higher simulated CO_2 surface flux, particularly under light-saturating conditions (not shown). Since a coupled model for stomatal conductance is used (see Eq. 8), an increase in CO_2 concentrations and carbon assimilation is linked with a decrease of stomatal conductance in the simulations (cf. Fig. 11a). This decline is strong for

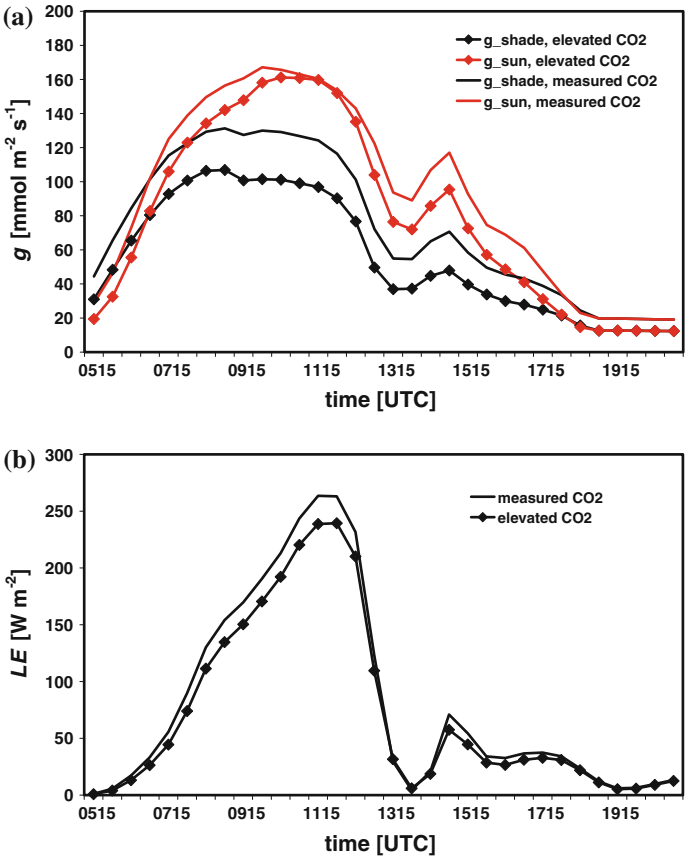

Fig. 11 Simulated 30-min averaged stomatal conductance (*upper panel*) and latent heat fluxes (*LE, lower panel*). Shown are results with measured ambient (*solid lines*) and elevated (*dotted lines*) atmospheric CO_2 concentrations for a grid point with wheat

the shaded fraction (black lines in Fig. 11a), while only a slight decrease is simulated for the sunlit leaves (red lines in Fig. 11a). Since the stomatal conductance of both fractions is used to compute the latent heat flux (see Eqs. 15 and 16), the reduced stomatal conductance results in a weakened simulated latent heat flux (*LE*) under elevated CO_2 (Fig. 11b). Around midday, when *LE* is highest, the elevated CO_2 leads to a decrease in *LE* of about 10%. A total of about 11% less transpirational water loss under elevated CO_2 is detected for the entire day. Thus, our results are consistent with the findings of e.g. Tricker et al. (2005) and Garcia-Amorena et al. (2006).

5 Discussion and Conclusions

In this study, we estimated the advantages of using a sun/shade model (de Pury and Farquhar 1997) compared to a big leaf model for the correct simulation of surface fluxes. With this aim, we coupled a mesoscale meteorological model (FOOT3DK) with a photosynthesis-based gas exchange model to simulate the fluxes of CO_2 and H_2O over an area with different land-use types. The transpiration of plants is linked to the photosynthesis by the use of a carbon assimilation-based stomatal model of Ball et al. (1987). By dividing the canopy into sunlit and shaded fractions (de Pury and Farquhar 1997), the stomatal conductances of the sunlit and shaded leaves are used to compute the transpirational water loss of the plants. The coupled model has been evaluated by comparing simulated latent heat fluxes and CO_2 net ecosystem exchange of single grid points with eddy-covariance measurements over fields with wheat and sugar beet. Main results are as follows:

- The stand-alone version of the gas exchange model simulates realistic net ecosystem exchange of CO_2. While the absolute values may differ in some cases, the general course of the day of net ecosystem exchange is well captured by the model.
- The application of the Jarvis-type big leaf approach in the land-surface scheme leads to a systematic overestimation of the latent heat fluxes, a common feature of mesoscale numerical models using this approach (e.g. Maurer and Heinemann 2006; Mengelkamp et al. 2006).
- By replacing the Jarvis-type scheme by a photosynthesis-based scheme for stomatal conductance, latent heat fluxes are simulated more realistically, particularly during spring time. During summer, only small differences between both schemes are observed. In most studies that investigate the correspondence between the fluxes of CO_2 and H_2O, the coupled ecosystem models are forced with observed meteorological data (e.g. Houborg and Soegaard 2004; Kothavala et al. 2005). The meteorological variables in our coupled model are predicted by the atmospheric component of FOOT3DK, thus enabling the simulation of scenarios for complete landscapes.
- For simulated time-averaged latent heat fluxes and net ecosystem exchange over different land-use types a moderate anticorrelation is observed. A higher anticorrelation is found for the net ecosystem exchange and transpirational water loss, reflecting the fact that both fluxes are linked by the stomatal conductance.
- Regarding the relationship between surface characteristics and the fluxes of CO_2 and H_2O, the simulations reveal a high correlation between net ecosystem exchange and LAI. On the other hand, the correlation between the latent heat flux and LAI is much weaker. These results are consistent with observational studies: e.g. Górska et al. (2008) detected a correlation between LAI and latent heat fluxes of only 0.32, while the correlation of the LAI with CO_2 fluxes was much higher ($r = 0.7$).

– With elevated atmospheric CO_2 concentration the simulated stomatal conductance is reduced, resulting in a decrease in the transpirational water loss and thus of the latent heat flux. These results agree well with other studies (e.g. Tricker et al. 2005; Garcia-Amorena et al. 2006). Of course, the response of the stomatal conductance to elevated atmospheric CO_2 is complex and is determined by many environmental (Konrad et al. 2008) and plant internal factors (e.g. acclimation), as well as feedback processes at the ecosystem scale (e.g. Norby and Luo 2004; Atkin et al. 2005). Nevertheless, the coupled model may provide a valuable tool for assessing potential changes in ecosystem-atmosphere exchange under future climate scenarios.

The benefit of using photosynthesis-based land-surface schemes in mesoscale meteorological models has been recently pointed out by several studies. Niyogi et al. (2009) for example developed a coupled photosynthesis-based gas exchange evapotranspiration model for application in mesoscale weather forecast models. In their coupled model a big leaf approach is used, and they suggested that in high resolution models and/or for tall canopies a detailed sun/shade scaling might be used. In the present study we demonstrated that the coupled model is indeed able to capture the surface fluxes of two land-use types (wheat and sugar beet). For further investigations, the model evaluation for other land-use types is necessary. Nevertheless, the results of the present study demonstrate that the use of a photosynthesis-based sun/shade gas exchange model leads to more realistic latent heat fluxes. Therefore, we suggest that photosynthesis-based sun/shade gas exchange models could be applied in forecast models and in future studies with mesoscale models.

Acknowledgments This research was supported by the Transregional Collaborative Centre 32 "Pattern in Soil-Vegetation-Atmosphere Systems: Monitoring, Modelling, and Data Assimilation" (Transregio/SFB32), funded by the Deutsche Forschungsgemeinschaft (DFG). Thanks for providing observations go to TR32 participants Alexander Graf and Anke Schickling, and to Marius Schmidt of the University of Cologne. We gratefully acknowledge Guido Waldhoff of the TR32 project "Database and Data Management" for preparing the land-use classification. The authors thank three anonymous reviewers for their detailed comments and suggestions.

References

Adegoke JO, Pielke R, Carleton AM (2007) Observational and modelling studies of the impacts of agricultural-related land use change on planetary boundary layer processes in the central US. Agric For Meteorol 142:203–215

Atkin OK, Bruhn D, Hurry VM, Tjoelker MG (2005) The hot and the cold: unravelling the variable response of plant respiration to temperature. Funct Plant Biol 32:87–105

Baldauf M, Förstner C, Klink S, Reinhardt T, Schraff C, Seiffert A, Stephan K (2009) Kurze Beschreibung des Lokal-Modells Kürzesfrist COSMO-DE (LMK) und seiner Datenbank auf dem Datenserver des DWD. Deutscher Wetterdienst, Geschäftsbereich Forschung und Entwicklung, Offenbach, Germany, 72 pp

Ball JT, Woodrow IE, Berry JA (1987) A model predicting stomatal conductance and its contribution to the control of photosynthesis under different environmental conditions. In Biggens J (ed) Progress in photosynthesis research IV. Martinus Nijhoff, Dordrecht, pp 221–224

Beyrich F, Mengelkamp HT (2006) Evaproation over heterogeneous land surface: EVA_GRIPS and the LITFASS-2003 experiment—an overview. Boundary-Layer Meteorol 121:5–32

Beyschlag W, Ryel RJ (1999) Canopy modelling. In: Pugnaire F, Valladares F (eds) Handbook of plant functional ecology. Marcel Dekker, New York, pp 771–804

Bonan GB (1995) Land–atmosphere CO_2 exchange simulated by a land surface process model coupled to an atmospheric general circulation model. J Geophys Res 100:2817–2831

Brücher W (1997) Numerische Studien zum Mehrfachnesting mit einem nicht-hydrostatischen modell. Dissertation, University of Cologne
Brücher W, Kerschgens M, Steffany F (1994a) On the generation of synthetic wind roses in orographocally structured terrain. Theor Appl Climatol 48:203–207
Brücher W, Kerschgens M, Steffany F (1994b) Synthetik wind climatologies. Meteorol Z 3:183–186
Brücher W, Kessler C, Kerschgens M, Ebel A (2001) Simulation of traffic-induced air pollution on regional to local scales. Atmos Environ 34(27):4675–4681
Bunnell FL, Tait DEN, Flanagan PW, Van Cleve K (1977) Microbial respiration and substrate weight loss, I, A general model of the influences of abiotic variables. Soil Biol Biochem 9:33–40
Collatz GJ, Ball JT, Griver C, Berry JA (1991) Physiological and environmental regulation of stomatal conductance, photosynthesis and transpiration: a model that includes a laminar boundary layer. Agric For Meteorol 54:107–136
Dai Y et al (2003) The common land model. Bull Am Meteorol Soc 84:1013–1023
de Arellano JVG, Gioli B, Miglietta F, Jonker HJJ, Baltink HK, Hutjes RWA, Holtslag AAM (2004) The entrainment process of carbon dioxide in the atmospheric boundary layer. J Geophys Res 109:110–124
de Pury DGG, Farquhar GD (1997) Simple scaling of photosynthesis from leaves to canopies without the errors of big-leaf models. Plant Cell Environ 20:537–557
Farquhar GD, von Caemmerer S, Berry JA (1980) A biochemical model of photosynthetic CO_2 assimilation in leaves of C_3 species. Planta 149:78–90
Fesquet C, Drobinski P, Barthlott C, Dubos T (2009) Impact of terrain heterogeneity on near-surface turbulence structure. Atmos Res 94:254–269
Garcia-Amorena I, Wagner F, van Hoof TB, Gomez Manzaneque FG (2006) Stomatal responses in deciduous oaks from southern Europe to the anthropogenic atmospheric CO_2 increase; refining the stomatal-based CO_2 proxy. Rev Palaeobot Palynol 141:303–312
Górska M, Vilà-Gueraude Arellano J, LeMone MA, van Heerwarden CC (2008) mean and flux horizontal variability of virtual potential temperature, moisture, and carbon dioxide: aircraft observations and LES study. Mon Weather Rev 136:4435–4451
Graf A, Prolingheuer N, Schickling A, Schmidt M, Schneider K, Schüttemeyer D, Herbst M, Huisman JA, Weihermüller L, Scharnagl B, Steenpass C, Harms R, Vereecken H (2010a) Temporal downscaling of soil CO_2 efflux measurements based on time-stable spatial patterns. Vadose Zone J. doi:10.2136/vzj2009.0152
Graf A, Schüttemeyer D, Geiß H, Knaps A, Möllmann-Coers M, Schween JH, Kollet S, Neininger B, Herbst M, Vereecken H (2010b) Boundedness of turbulent temperature probability distributions, and their relation to the vertical profile in the convective boundary layer. Boundary-Layer Meteorol 134:459–486
Harley PC, Thomas RB, Reynolds JF, Strain BR (1992) Modelling photosynthesis of cotton grown in elevated CO_2. Plant Cell Environ 15:271–282
Heinemann G, Kerschgens M (2005) Comparison of methods for area-averaging surface energy fluxes over heterogenous land surfaces using high-resolution non-hydrostatic simulations. Int J Climatol 25:379–403. doi:10.1002/joc.1123
Houborg RM, Soegaard H (2004) Regional simulation of ecosystem CO_2 and water vapor exchange for agricultural land using NOAA AVHRR and Terra MODIS satellite data. Application to Zealand, Denmark. Remote Sens Environ 93:150–167
Hübener H, Schmidt M, Sogalla M, Kerschgens M (2005) Simulating evapotranspiration in a semi-arid environment. Theor Appl Climatol 80:153–167
Jacobsen I, Heise E (1982) A new economic method for the computation of the surface temperature in numerical models. Beitr Phys Atmos 55:28–41
Jarvis P (1976) The interpretation of leaf water potential and stomatal conductance found in canopies in the field. Philos Trans R Soc Lond Ser B Biol Sci 273:593–610
Konrad W, Roth-Nebelsick A, Grein M (2008) Modelling of stomatal density response to atmospheric CO_2. J Theor Biol 253:638–658
Kothavala Z, Arain MA, Black TA, Verseghy D (2005) The simulation of energy, water vapor and carbon dioxide fluxes over common crops by the Canadian Land Surface Scheme (CLASS). Agric For Meteorol 133:89–108
Kvifte G, Hegg K, Hansen V (1983) Spectral distribution of solar radiation in the Nordic countries. J Clim Appl Meteorol 22:143–152
LeMone MA, Chen F, Alfieri JG, Tewari M, Geerts B, Miao Q, Grossman RL, Coulter RL (2007) Influence of land cover and soil moisture on the horizontal distribution of sensible and latent heat fluxes in southeast Kansas during IHOP_2002 and CASES-97. J Hydrometeorol 8:68–87

Maurer B, Heinemann G (2006) Validation of the "Lokal-Modell" over heterogeneous land surfaces using aircraft-based measurements of the REEEFA experiment and comparison with micro-scale simulations. Meteorol Atmos Phys 91:107–128

Mengelkamp HT, Beyrich F, Heinemann G, Ament F, Bange J, Berger F, Bösenberg J, Foken T, Hennemuth B, Heret C, Huneke S, Johnsen KP, Kerschgens M, Kohsiek W, Leps JP, Liebethal C, Lohse H, Maider M, Meijninger W, Raasch S, Simmer C, Spiess T, Titterbrand A, Uhlenbrock J, Zittel P (2006) Evaporation over a heterogeneous land surface—the EVA-GRIPS Project. Bull Am Meteorol Soc 87:775–786

Niyogi D, Alapaty K, Raman S, Chen F (2009) Development and evaluation of a coupled photosynthesis –based gas exchange evapotranspiration model (GEM) for mesoscale weather forecasting applications. J Appl Meteorol Climatol 48:349–368

Noilhan J, Planton S (1989) A simple parameterization of land surface processes for meteorological models. Mon Weather Rev 117:536–549

Norby RJ, Luo Y (2004) Evaluating ecosystem responses to rising atmospheric CO_2 and global warming in a multi-factor world. New Phytol 162:281–293

Pielke RA, Avissar R (1990) Influence of landscape structure on local and regional climate. Landsc Ecol 4:133–155

Pielke RA, Niyogi D (2009) The role of landscape processes within the climate system. In: Otto JC, Dikaum R (eds) Landform-structure, evolution, process control: proceedings of the international symposium on Landforms organised by the research training group 437, vol 115. Springer, Berlin, 67 pp

Pinto JG, Neuhaus CP, Krüger A, Kerschgens M (2009) Assessment of the wind gust estimates method in mesoscale modelling of storm events over West Germany. Meteorol Z 18:495–506

Ryel RJ, Beyschlag W, Caldwell MM (1993) Foliage orientation and carbon gain in two tussock grasses as assessed with a new whole-plant gas-exchange model. Funct Ecol 7:115–124

Sellers PJ, Berry JA, Collatz GJ, Field CB, Hall FG (1992) Canopy reflectance, photosynthesis, and transpiration. III. A reanalysis using improved leaf models and a new canopy integration scheme. Remote Sens Environ 42:187–216

Sellers PJ et al. (1996) A revised land surface parameterisation (SiB2) for atmospheric GCMs. Part I: model formulation. J Clim 9:676–705

Shao Y, Sogalla M, Kerschgens M, Brücher W (2001) Effects of land-surface heterogeneity upon surface fluxes and turbulent conditions. Meteorol Atmos Phys 78:157–181

Sogalla M, Krüger A, Kerschgens M (2006) Mesoscale modelling of interactions between rainfall and the land surface in West Africa. Meteorol Atmos Phys 91:211–221

Szeicz G (1974) Solar radiation for plant growth. J Appl Ecol 11:617–636

Tricker PJ, Trewin H, Kull O, Clarkson GJJ, Eensalu E, Tallis MJ, Colella A, Doncaster CP, Sabatti M, Taylor G (2005) Stomatal conductance and not stomatal density determines the long-term reduction in leaf transpiration of poplar in elevated CO_2. Oecologia 143:652–660

Waldhoff G (2010) Land use classification of 2009 for the Rur catchment. doi:10.1594/GFZ.TR32.1

Werner C, Correia O, Ryel RJ, Beyschlag W (2001) Effects of photoinhibition on whole-plant carbon gain assessed with a photosynthesis model. Plant Cell Environ 24:27–40

Xiu A, Pleim JE (2001) Development of a land surface model, part I: application in a mesoscale meteorological model. J Appl Meteorol 40:192–209

Zhan X, Kustas WP (2001) A coupled model of land surface CO_2 and energy fluxes using remote sensing data. Agric For Meteorol 107:131–152